doi:10.1016/j.jmb.2007.08.049 J. Mol. Biol. (2007) 373, 1198–1212

JMB

Available online at www.sciencedirect.com
ScienceDirect

ELSEVIER

Interactions between the Leucine-zipper Motif of cGMP-Dependent Protein Kinase and the C-terminal Region of the Targeting Subunit of Myosin Light Chain Phosphatase

Eunhee Lee[1], David B. Hayes[1], Knut Langsetmo[1], Eric J. Sundberg[1] and Terence C. Tao[1,2,3]*

[1]*Cardiovascular Program Boston Biomedical Research Institute, Watertown MA 02472, USA*

[2]*Department of Neurology Harvard Medical School Boston, MA 02115, USA*

[3]*Department of Biochemistry Tufts University School of Medicine, Boston, MA 02111 USA*

Received 20 April 2007; received in revised form 12 July 2007; accepted 21 August 2007
Available online 25 August 2007

Edited by J. E. Ladbury

Nitric oxide induces vasodilation by elevating the production of cGMP, an activator of cGMP-dependent protein kinase (PKG). PKG subsequently causes smooth muscle relaxation in part *via* activation of myosin light chain phosphatase (MLCP). To date, the interaction between PKG and the targeting subunit of MLCP (MYPT1) is not fully understood. Earlier studies by one group of workers showed that the binding of PKG to MYPT1 is mediated by the leucine-zipper motifs at the N and C termini, respectively, of the two proteins. Another group, however, reported that binding of PKG to MYPT1 did not require the leucine-zipper motif of MYPT1. In this work we fully characterized the interaction between PKG and MYPT1 using biophysical techniques. For this purpose we constructed a recombinant PKG peptide corresponding to a predicted coiled coil region that contains the leucine-zipper motif. We further constructed various C-terminal MYPT1 peptides bearing various combinations of a predicted coiled coil region, extensions preceding this coiled coil region, and the leucine-zipper motif. Our results show, firstly, that while the leucine-zipper motif at the N terminus of PKG forms a homodimeric coiled coil, the one at the C terminus of MYPT1 is monomeric and non-helical. Secondly, the leucine-zipper motif of PKG binds to that of MYPT1 to form a heterodimer. Thirdly, when the leucine-zipper motif of MYPT1 is absent, the PKG leucine-zipper motif binds to the coiled coil region and upstream segments of MYPT1 *via* formation of a heterotetramer. These results provide rationalization of some of the findings by others using alternative binding analyses.

Keywords: smooth muscle; myosin phosphatase; protein kinase G; analytical ultracentrifugation; surface plasmon resonance

Introduction

Smooth muscle contraction is regulated primarily by intracellular Ca^{2+}.[1,2] Elevation of the cytosolic Ca^{2+} level activates calmodulin, which then activates myosin light chain kinase (MLCK). MLCK phosphorylates the 20 kDa regulatory myosin light chain (MLC_{20}) at residues Ser19 and Thr18, whereupon myosin ATPase activity is activated, leading to contraction.[1] By measuring the cytosolic Ca^{2+} concentration and force development simultaneously, it was discovered that the Ca^{2+} sensitivity of contraction varied depending on the nature of the stimulation.[2–5] At a given fixed Ca^{2+} level, different

*Corresponding author. E-mail address: Tao@BBRI.org.

Abbreviations used: MLCK, myosin light chain kinase; MLC_{20}, 20 kDa regulatory light chain of myosin; MLCP, human aorta myosin light chain phosphatase; PP1cδ, MYPT1 and M21, the catalytic, targeting and small subunits of MLCP, respectively; PKG, cGMP-dependent protein kinase, the PKGIα isoform; RU, resonance unit(s); M, molar mass; MW, molecular weight; T_m, temperature midpoint for thermal denaturation. *s*, the sedimentation coefficient; *s**, the apparent sedimentation coefficient; *g*(*s**), the distribution function for *s**.

types of stimulation induced various levels of tension. Thus, both the Ca^{2+} signal and the alteration of the Ca^{2+} sensitivity of the contractile apparatus are involved in the regulation of smooth muscle contraction.

Myosin light chain phosphatase (MLCP) dephosphorylates MLC_{20}, causing smooth muscle relaxation.[6,7] MLCP consists of a 38 kDa catalytic subunit (PP1cδ), a 110 kDa targeting subunit (MYPT1), and a 21 kDa small subunit (M21) whose function is unknown. MYPT1 activates the activity of PP1cδ, and imparts substrate specificity of MLCP toward myosin filaments. The level of MLC_{20} phosphorylation is determined by the balance between the activities of MLCK and MLCP. In smooth muscle, intracellular messengers regulate the Ca^{2+} sensitivity of the contractile apparatus by modulating MLCP activity. RhoA,[8] protein kinase C,[9] and arachidonic acid[10] increase MLC_{20} phosphorylation by inhibiting MLCP. RhoA activates Rho kinase, which subsequently phosphorylates MYPT1 and inhibits MLCP activity.[8] Protein kinase C inhibits MLCP activity by phosphorylating and thereby activating CPI-17, which inhibits MLCP activity.[9,11,12] Arachidonic acid inhibits MLCP activity, possibly by dissociating MLCP subunits[10] and/or by activating Rho kinase.[13]

Nitric oxide increases the production of the second messenger cGMP, decreases MLC_{20} phosphorylation and causes smooth muscle relaxation by reducing intracellular Ca^{2+} as well as Ca^{2+}-sensitivity of the contractile apparatus. cGMP activates the cGMP-dependent protein kinase (PKG) and decreases intracellular Ca^{2+} through several mechanisms, including phosphorylation of the thromboxane receptor,[14] phospholamban[15] and the inositol triphosphate receptor and/or IRAG.[16–19] cGMP also modulates the potassium[20,21] and L-type calcium channels.[22,23] cGMP reduces the Ca^{2+} sensitivity of the contractile apparatus by activating MLCP[24–29] through a mechanism that is not well understood because phosphorylation of MYPT1 by PKG has no effect on the activity of MLCP.[30] A possible mechanism was suggested by Wooldridge *et al.*,[31] who reported that phosphorylation of MYPT1 at Thr695 by PKG suppressed phosphorylation by other kinases such as Rho kinase at the Thr696 inhibitory site of MYPT1. Thus, cGMP and PKG may exert an apparent activation effect by suppressing an inhibitory pathway of MLCP.[31] It has been reported that PKG binds directly to MYPT1, and that this binding is required for optimal activation of MLCP activity.[32] These authors also reported that this binding is mediated by the leucine-zipper motifs at the N and C-terminal regions of PKG and MYPT1, respectively.[28,32] A study using permeabilized smooth muscle strips appears to be consistent with these observations; whereas tissues that express the MYPT1 isoform that contains the leucine-zipper motif (chicken aorta and embryonic gizzard) are capable of relaxing in response to 8-bromo-cGMP, an analogue of cGMP, those expressing the leucine-zipper-absent MYPT1 isoform (mature chicken gizzard) are insensitive to 8-bromo-cGMP.[27] However, a more recent study showed that the binding of PKG to MYPT1 required neither cGMP nor the leucine-zipper motif at the C terminus of MYPT1, although the MYPT1 leucine-zipper motif was needed for cGMP-mediated smooth muscle relaxation.[29] Very recently it was reported that the RK motif at residues 916–917 in the residues 888–928 region of MYPT1 mediates binding to PKG.[33] Thus, neither the mechanism whereby PKG activates MLCP, nor the nature of the interaction between these two proteins are completely understood.

Here, we used biophysical techniques to fully characterize the interaction of the C-terminal region of MYPT1 with the N-terminal leucine-zipper motif of PKG. We used these peptide fragments because they could be expressed in large quantities necessary for these studies, and because studies by Surks *et al.* had shown that deletion mutants that do not contain residues 1–59 of PKG did not bind MYPT1, while those that do, including this region itself, bound to MYPT1.[32] They further reported that whereas the 690 residues N-terminal portion of MYPT1 did not bind PKG, the residues 850–1030 C-terminal portion (corresponding to the fragment designated as E_1E_2CCLZ in this study; see below) did bind PKG.[32] Aside from the leucine-zipper motif, the C-terminal region of MYPT1 contains a predicted (by the online sequence analysis program MULTICOIL[34]) coiled coil†‡ region that may serve as an alternate binding site for PKG. Accordingly, we expressed and purified various C-terminal MYPT1 peptides that contain either the leucine-zipper, or the coiled coil or both motifs, as well as a PKG peptide that contains its N-terminal leucine-zipper motif (see the list in Figure 1). We characterized the individual peptides using circular dichroism spectrometry and analytical ultracentrifugation. We then examined the interactions between the MYPT1 peptides and the PKG peptide using analytical ultracentrifugation and surface plasmon resonance. As discussed, our results

†We define a coiled coil region as one that contains tandem heptad repeats in which the first and fourth residues (a and d residues, respectively) are hydrophobic. A leucine-zipper motif is a coiled coil region in which the a and d residues are either Leu or Ile.

‡In an earlier publication[35] we reported that the program PAIRCOIL predicted the presence of coiled coil regions at residues 674–705 and 888–928 in the 107 kDa isoform of chicken gizzard MYPT1 (which does not contain the 41 residues central insert), corresponding to residues 715–746 and 925–969 in the 115 kDa isoform of human aorta MYPT1 (containing both the central insert and the C-terminal LZ motif). Visual inspection of the first predicted coiled coil region revealed that the sequence does not contain any heptad repeats. Instead, the sequence resembles that of the highly α-helical segment in caldesmon.[36] Indeed, the program MULTICOIL, a later version of PAIRCOIL that was used in this previous work, does not predict this region to be a coiled coil.

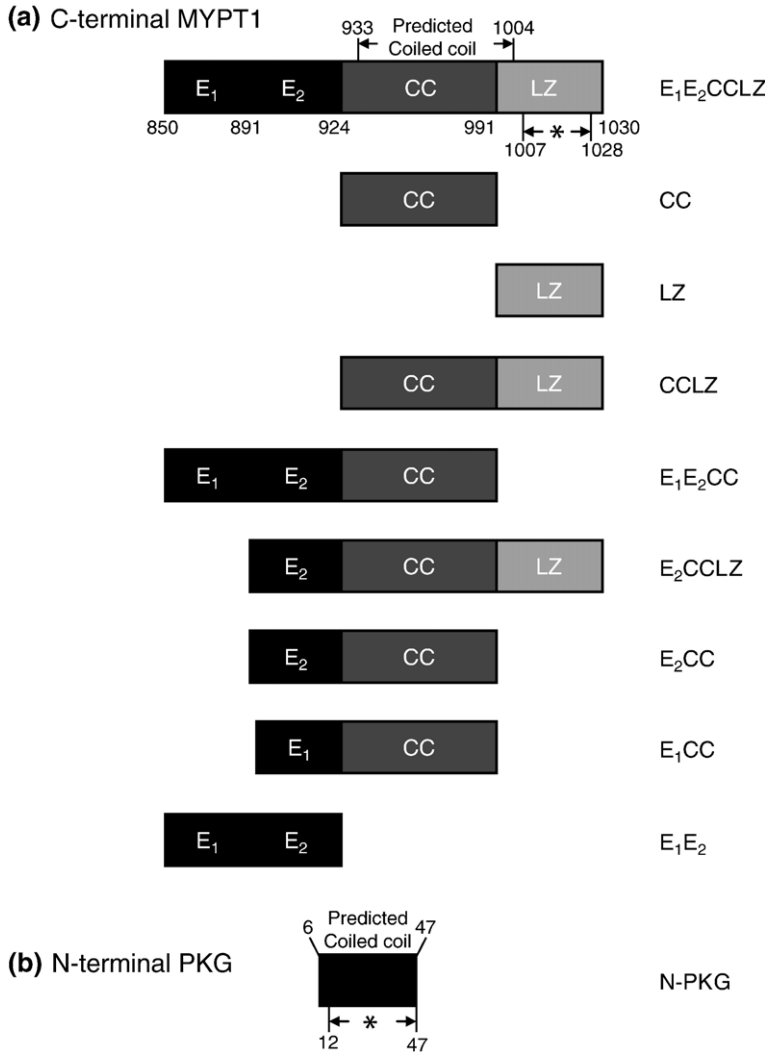

Figure 1. Schematic representation of the various C-terminal MYPT1 peptides and that of the N-terminal PKG peptide. (a) The C-terminal region of MYPT1 was divided into four segments designated as E_1, E_2, CC, and LZ. The predicted coiled coil region was indicated by the program MULTICOIL.[34] The asterisk denotes the leucine-zipper motif. (b) N-PKG comprises exclusively a predicted coiled coil region within which the leucine/isoleucine-zipper motif (also denoted with an asterisk) is located.

provide rationalization for most, but not all, of the findings reported in the literature.

Results

Construction, expression, and purification of the peptides

To map the PKG interaction region in MYPT1, we expressed various peptides corresponding to the C-terminal region of MYPT1. This region has a predicted coiled coil region (residues 933–1004), followed by the leucine-zipper motif (residues 1007–1028) (Figure 1(a)). We divided the C-terminal region of MYPT1, residues 850–1030, into four segments, *viz*. E_1, E_2, CC, and LZ (Figure 1(a)). CC contains most of the predicted coiled coil region, and LZ contains the leucine-zipper motif following the CC region. E_1 and E_2 represent two regions that are N-terminal extensions from the CC region. We expressed and purified eight MYPT1 peptides corresponding to various combinations of these four segments. As illustrated in Figure 1(a), the peptides are designated as CC, LZ, CCLZ, E_1E_2CC, E_2CCLZ, E_2CC, E_1CC, and E_1E_2 according to their compositions. The leucine-zipper motif of PKG spans residues 12–47, and is within a predicted coiled coil region comprising residues 6–47 (Figure 1(b)). The cDNA fragment encoding this predicted coiled coil region was amplified by PCR using a PKG cDNA clone that was obtained from a human aorta cDNA library (see Materials and Methods). The purity of all the peptides were verified by 16.5%(w/v) Tris-tricine polyacrylamide gel electrophoresis (data not shown), and their identities were confirmed by mass spectrometry.

Structural characterization of the peptides

The secondary structures of the purified N-PKG and MYPT1 peptides were determined by far-UV circular dichroism spectroscopy. As can be seen in Figure 2, these peptides contain varying amounts of α-helical structures; their estimated α-helix contents are summarized in the inset of Figure 2. Noticeably, N-PKG has 71% of α-helical content, whereas LZ contains only 6%, even though both peptides have the leucine/isoleucine heptad repeats of the leucine-zipper motif. As expected from sequence analysis, E_1E_2 has very low helix content. CC has an α-helical content of 56%, and other CC-containing MYPT1 peptides have reduced α-helix contents relative to CC, consistent with our finding that E_1, E_2, and LZ have very low α-helical contents.

To examine the thermodynamic stability of some of the peptides that have significant α-helical contents, *viz*. N-PKG, CC, E_1E_2CC, E_2CCLZ, and CCLZ, we performed thermal denaturation experiments by monitoring the ellipticity at 222 nm between 10 °C and 80 °C. Figure 3(a) shows the decrease in the normalized (by the value at 10 °C) ellipticity, corresponding to the decrease in α-helix content (increase in unfolding), for these peptides. CC and the three CC-containing peptides exhibit a slight decrease in the normalized ellipticity between 10 °C and ~40 °C, followed by a sharper decrease indicative of cooperative transition to the unfolded state. The transition midpoints, T_m, for these peptides were estimated from the maxima of the derivatives of the melting curves, and found to be roughly similar to each other (Figure 3(a), inset). To examine whether the peptides could be renatured after thermal denaturation, each peptide was cooled from 80 °C back to 10 °C and its circular dichroism spectrum rescanned. The rescanned spectra overlapped with those of the original scans, indicating that thermal denaturation of these peptides is fully reversible (data not shown). Without incubating with fresh DTT, N-PKG, which contains a single cysteine at position 42, shows no sharp increase in ellipticity in the entire temperature range. N-PKG treated with fresh 2 mM DTT exhibits the beginning of a transition at ~68 °C. These data indicate that reduced N-PKG is more stable than the CC-containing peptides, with a T_m value that lies higher than 80 °C, and that oxidized N-PKG is even more stable, most likely further stabilized by a disulfide bond at position 42.

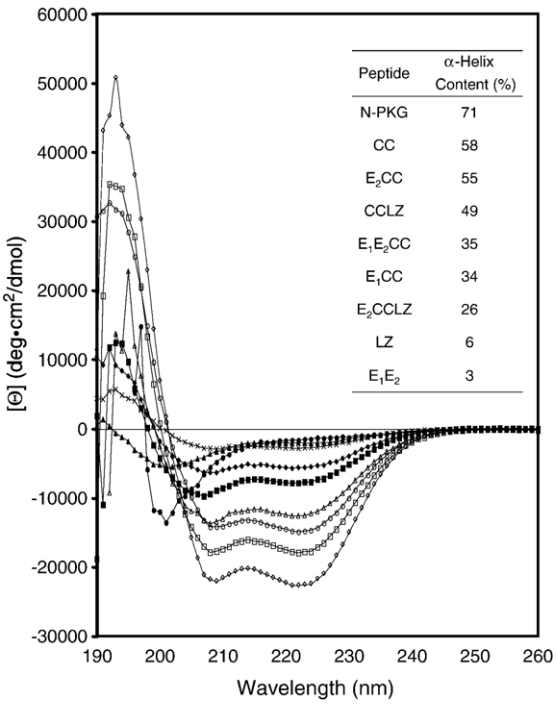

Figure 2. Circular dichroism spectra of the purified peptides. In descending order of α-helix content, the spectra (mean residue ellipticity *versus* wavelength) of N-PKG (open diamonds), CC (open rectangles), CCLZ (open circles), E_2CC (open triangles), E_1E_2CC (filled rectangles), E_1CC (filled diamonds), E_2CCLZ (crosses), LZ (filled triangles), and E_1E_2 (filled circles) are shown. Each spectrum represents an average of five scans collected at 25 °C, from a 0.5 mg/ml peptide solution in 5 mM potassium phosphate buffer (pH 8.0), containing 10 mM KCl, and 1 mM DTT. Smoothing functions were not applied to these spectra. Inset: α-Helix contents of the peptides, determined from the circular dichroism spectra in this Figure, and equation (2) in Materials and Methods. The reproducibility of the values are estimated to be 2% or better.

Differential scanning calorimetry experiments

Differential scanning calorimetry was used to determine the value of T_m for reduced N-PKG. A fit of the data in Figure 3(b) to a non-two-state model yielded a T_m of 94 °C, a calorimetric enthalpy of 23 kcal mol^{-1}, and a van't Hoff enthalpy of 55 kcal mol^{-1}. The data yielded a value of 2.4 for the ratio between the van't Hoff and calorimetric enthalpies, a value that is consistent with a folded dimer to unfolded monomers transition.[37] By assuming ΔCp to have typical values of between 10 and 500 cal mol^{-1} $°K^{-1}$,[38] the dissociation constant, K_d, for the N-PKG dimer could be estimated from the van't Hoff relationship to be between 0.05 and 1.0 μM, consistent with the value of 0.5 μM determined by analytical ultracentrifugation (see below).

Sedimentation velocity experiments

The self-association stoichiometry of each peptide was characterized by analytical ultracentrifugation sedimentation velocity experiments, using SEDANAL to analyze the data. Using the data for N-PKG at 92.8, 30.9 and 10.3 μM (prepared by threefold serial dilution) as examples, Figure 4(a) shows that the apparent sedimentation coefficient distribution function, $g(s^*)$, for N-PKG at 92.8 and 31.0 μM appears to be symmetric Gaussian functions, approaching zero at high s^* values. These qualitative observations suggest that N-PKG exists as a single species that is undergoing neither dissociation nor

oligomerization under these conditions. To confirm this notion and to obtain quantitative information, the time-difference curves (Δc *versus* radius) were fit globally with N-PKG modeled as a single species, and the values of the molar mass and sedimentation coefficient, s, allowed to float. The results show that the value of the molecular mass (11,526 Da) obtained from the best fit to the data (Figure 4(b)) corresponds well to the calculated molecular weight of dimeric N-PKG (11,132 Da) (Table 1), clearly showing that N-PKG is a dimer under these conditions. At the lowest concentration of 10.3 μM the $g(s^*)$ curves revealed some dissociation of the N-PKG dimer. Fitting these curves using a dimer to monomers dissociation model with the values of the molecular mass and s fixed, and K_d allowed to vary yielded $K_d = 0.5$ μM. Statistical analysis revealed that K_d has a 95% probability of being within the values of K_d (max) = 1.07 μM and K_d(min) = 0.22 μM. Table 1 summarizes the results for some of the other peptides using the same analysis. It can be seen that the determined molecular mass for CC and the CC-containing peptides in Table 1 correspond well to the calculated molecular weights for their dimers. In contrast, the molecular mass for E_1E_2 corresponds well to the molecular weight for a monomer. For LZ this procedure could only be applied to the sample at the lowest concentration (see below). Doing so yielded a determined molecular mass that corresponds well to the molecular weight of a monomer (Table 1).

For LZ at the two higher concentrations, and the two LZ-containing peptides, E_2CCLZ and CCLZ, at all concentrations, boundary spreading towards higher s^* values was observed, giving rise to non-symmetric plots of the apparent sedimentation coefficient distribution function. This indicates the presence of higher-order oligomers in these samples. Since the nature of these oligomers are unknown, the stoichiometry of these two peptides could not be determined by the analysis outlined above. However, as will be discussed, our circular dichroism results and the fact that all the other CC-containing peptides are dimeric strongly suggest that E_2CCLZ and CCLZ are dimeric as well.

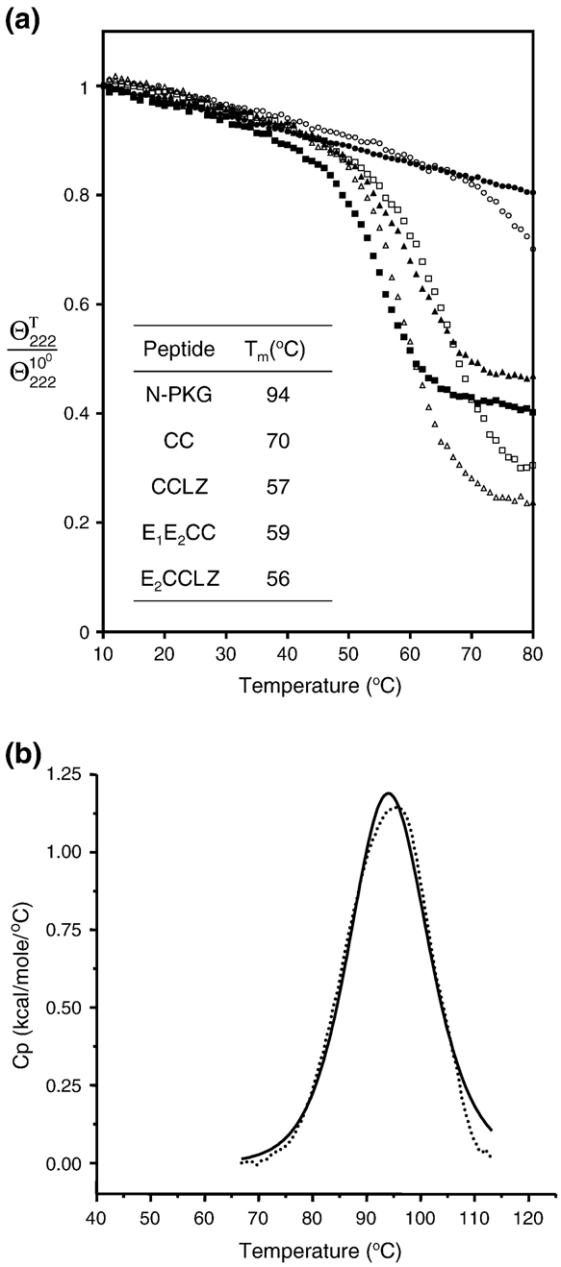

Figure 3. Thermal denaturation of N-PKG and MYPT1 peptides. (a) Relative amounts of folded peptides as measured by the ellipticity at 222 nm (normalized by the value at 10 °C), as the temperature was increased from 10 °C to 80 °C. Measurements were made on 0.05 mg/ml peptide solutions in 5 mM potassium phosphate buffer (pH 8.0), containing 10 mM KCl, and 1 mM DTT, except for N-PKG/DTT which was incubated with 2 mM DTT at 37 °C for 10 min just before measurements were taken. N-PKG (filled circles); N-PKG/DTT (open circles); CCLZ (open triangles); E_1E_2CC (filled triangles); E_2CCLZ (filled rectangles); CC (open rectangles). Inset: Transition midpoints, T_m, of thermal melting determined from the derivatives of the circular dichroism melting profiles, with the exception of N-PKG, for which differential scanning calorimetry (see (b)) was employed. The reproducibility in the values of T_m are estimated to be 3% or better. (b) Excess heat capacity of N-PKG as a function of temperature measured by differential scanning calorimetry. 50 μM N-PKG was dialyzed against 50 mM potassium phosphate buffer (pH 8.0), containing 100 mM KCl and 0.2 mM Tris (2-carboxyethyl)phosphine hydrochloride. Using the dialysis buffer as reference, the N-PKG sample was heated at a rate of 90 °C/h. After subtracting the baseline, the data were fit with the non-two state model using the function provided in Origin 7 (Microcal Inc., Northampton MA). Broken line, experimental points; continuous line, best fit to the data.

Binding of the MYPT1 peptides to N-PKG using analytical ultracentrifugation

To examine the interactions between N-PKG and the 8 MYPT1 peptides, we performed velocity analytical ultracentrifugation experiments on mixtures of the peptides at various concentrations. Representative $g(s^*)$ plots for some of these mixtures

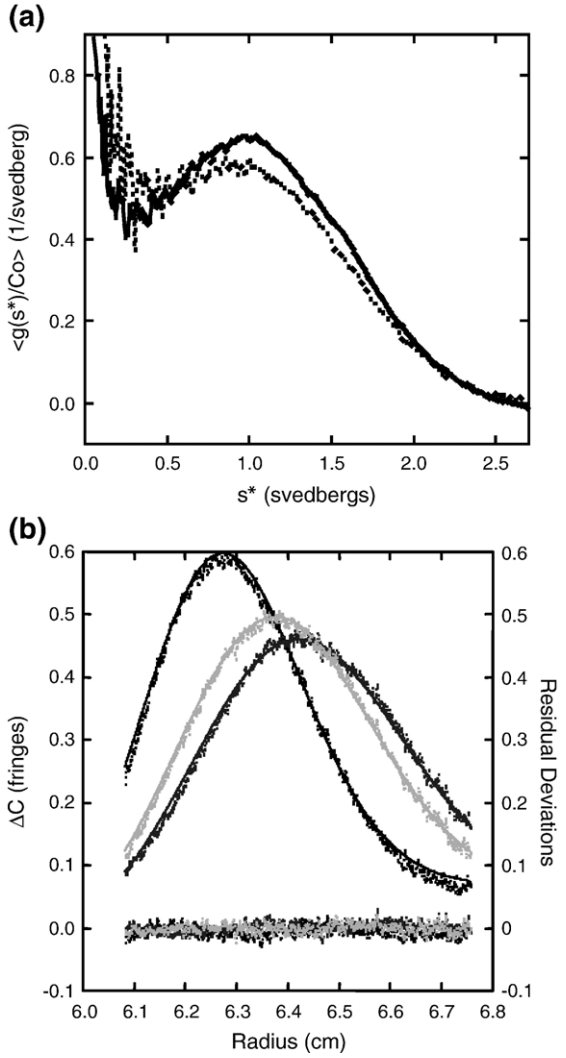

Figure 4. Sedimentation velocity analysis of N-PKG. (a) $g(s^*)$ plots for N-PKG at 92.8 (continuous line) and 31.0 μM (broken line), in 5 mM potassium phosphate buffer (pH 8.0), containing 100 mM KCl and 1 mM DTT (concentrations of these and all other samples are based on monomer molecular weights). Other conditions are specified in Materials and Methods. (b) Fitting of time-difference plots for N-PKG. A global fit of 900 total interference scans, 300 each at N-PKG concentrations of 92.8, 31.0 and 10.3 μM in the same buffer as described above, revealed that N-PKG is a dimer. Shown are three representative Δc *versus* radius plots used in the fitting, for a sample of N-PKG at 92.8 μM. The points are observed concentration differences at constant radius between two interference scans taken at different times, ΔC(obs). The continuous lines are concentration differences calculated using the parameters obtained from the best fit to the data, ΔC(cal). Also plotted are the deviations between ΔC(obs) and ΔC(cal), demonstrating the quality of the fits. The *x*-axis is the radius of the cell.

are shown in Figure 5. Figure 5(a) shows the $g(s^*)$ plot for an equimolar mixture of E_1E_2 and N-PKG, superimposed with those for N-PKG and E_1E_2 alone. It can be seen that the curve for the mixture is at the same position as that for E_1E_2 alone, suggesting that no complexation with E_1E_2 took place. This was confirmed using SEDANAL with a non-interacting model; the curve for the mixture could be fit by the sum of the curves for N-PKG and E_1E_2 alone (S.D. = 0.007), with the concentrations of the two peptides as floating parameters. Similar results were obtained for E_1CC and E_2CC. The peak of the $g(s^*)$ curve for an equimolar mixture of N-PKG and E_1E_2CC appears at a higher s^* value than both that of N-PKG and E_1E_2CC alone (Figure 5(b)), indicating the formation of a complex that sediments faster (has a higher molecular mass, assuming that the frictional ratios are similar) than both the N-PKG dimer (MW = 11,132 kDa) and the E_1E_2CC dimer (MW = 33,864 Da). The most likely complex is the $(E_1E_2CC)_2$–$(N\text{-}PKG)_2$ heterotetramer (MW = 44,996 Da), although the N-PKG–$(E_1E_2CC)_2$ heterotrimer (MW = 39,430 Da) is also possible (the $(N\text{-}PKG)_2$–E_1E_2CC heterotrimer (MW = 28,064 Da) is not likely because it would sediment slower than the $(E_1E_2CC)_2$ dimer). Further sedimentation velocity experiments were carried out with equimolar mixtures of these peptides at 21.6 μM, and the $g(s^*)$ plots were analyzed using SEDANAL with the molecular mass fixed at the calculated molecular weight of the heterotetramer, and the sedimentation coefficient and the concentrations allowed to float. As shown in Figure 5(c), the data could be fit adequately with a heterotetramer model (S.D. = 0.009), although the data could not rule out the aforementioned E_1E_2CC–$(N\text{-}PKG)_2$ heterotrimer model (S.D. = 0.01). The $g(s^*)$ curve for an equimolar mixture of E_2CCLZ and N-PKG revealed the formation of a complex that sediments faster then the N-PKG dimer and slower than the E_2CCLZ dimer (Figure 5(d)). The most likely complex is the N-PKG–E_2CCLZ heterodimer (MW = 22,423 kDa), whose molecular weight lies between those of the E_2CCLZ and the N-PKG dimers. Because the molecular weights of LZ and N-PKG are nearly the same, it was not possible to detect binding between these two peptides at low LZ concentrations. At a higher concentration, LZ forms oligomers that sediment at higher s^* values (Figure 5(e)). Addition of N-PKG to LZ under this condition produced a species that sediments slightly faster than LZ (Figure 5(e)), suggesting the binding of N-PKG to LZ oligomers. Clearly further characterization of this interaction using analytical ultracentrifugation could not be carried out. Analytical ultracentrifugation experiments on the binding of N-PKG with CC and with CCLZ yielded inconclusive results because the molecular weights of these two peptides are so small that the $g(s^*)$ curves for their complexes with N-PKG could not be distinguished from that of N-PKG alone.

Binding studies using surface plasmon resonance

Surface plasmon resonance was used to obtain quantitative information on the binding between N-PKG and some of the MYPT1 peptides, and to

Table 1. Characterization of purified peptides by velocity sedimentation analytical ultracentrifugation

Peptide	M_{cal} of monomer [dimer] (Dalton)	Standard deviation (Fringe)	M_{exp} (Dalton)			$S_{20,W}$	f/f_o
			M_{min}	M_{best}	M_{max}		
N-PKG	5566 [11,132]	0.006	11,180	11,526	11,871	1.26±0.01	1.41
CC	8490 [16,980]	0.006	18,397	18,966	19,535	1.40±0.01	1.68
E_1CC	12,569 [25,138]	0.010	22,691	22,994	23,300	1.72±0.01	1.91
E_2CC	12,178 [24,356]	0.010	23,183	23,342	23,499	1.72±0.01	1.82
E_1E_2CC	16,932 [33,864]	0.006	30,279	31,196	32,251	1.84±0.01	2.05
E_1E_2	8869 [17,738]	0.004	9456	9701	9950	1.05±0.01	1.73
LZ	5093 [10,186]	0.006	4582	4829	5089	0.71±0.01	1.43

Individual peptides were subjected to sedimentation velocity experiments as described in Materials and Methods. For global fits using SEDANAL, data from three or four serial dilutions of the peptides were analyzed, assuming a single species model. For LZ, only the lowest concentration was used because of self-association. M_{cal} is the calculated MW. M_{exp} is the experimentally determined molar mass: M_{best}, is the value of M_{exp} that yielded the best fit to the data; statistical analysis yielded a 95% probability that the value of M_{exp} falls between M_{min} and M_{max}. $S_{20,W}$ is the best fit sedimentation coefficient, corrected to 20 °C in water using SEDNTERP. f/f_o is the frictional ratio, the ratio between f, the frictional coefficient computed from the experimentally determined $S_{20,W}$ value, and f_o, the frictional coefficient of a sphere having the same molecular weight and partial specific volume as the peptide. The uncertainties in $S_{20,W}$ were derived from the fitting, and are all about or below 0.01. Because f/f_o was calculated from $S_{20,W}$, the percent error in it is equal to the percent error in $S_{20,W}$.

clarify inconclusive results from the analytical ultracentrifugation experiments. Since our sedimentation velocity results showed that there is no interaction between E_1CC and N-PKG, E_1CC was used as a control for non-specific binding. A nebulin peptide spanning residues 1624–1663, which is similar to LZ in size but is not expected to bind to N-PKG, was also used as a mock peptide for non-specific interaction. Because N-PKG could not be immobilized on the chips efficiently, the experiments were carried out with the MYPT1 peptides immobilized on the chips as the ligands, and N-PKG at serially diluted concentrations flowed through the cell as the analyte. Representative sensorgrams from our binding studies show that E_1CC (data not shown), E_1E_2CC and CC do not bind to N-PKG (Figure 6(a)). This is likely to be due to the fact that after washing of the immobilized peptides with buffer, the conditions were equivalent to that of infinite dilution, so that only one of the two chains is likely to remain immobilized on the chip, and our analytical ultracentrifugation results for E_1E_2CC demonstrated that dimeric peptides are required to bind to N-PKG. In contrast, E_2CCLZ, CCLZ, and LZ showed concentration-dependent binding to N-PKG (Figure 6(a)). Because the reaction we are dealing with here involves multiple equilibria (dissociation of $(\text{N-PKG})_2$ followed by binding to the immobilized peptide) the binding data could not be analyzed by the standard analysis software provided by Biacore. Using LZ, which is monomeric under these conditions, as an example, the steady-state binding curve (Figure 6(b)), was analyzed using the following reaction scheme:

$$\text{N-PKG}\bullet\text{N-PKG} = 2\text{N-PKG} \quad K_d = 0.5 \times 10^{-6}\text{M}$$

$$\text{LZ}^* + \text{N-PKG} = \text{N-PKG}\bullet\text{LZ}^* \quad K_a = ?$$

where LZ* denotes the immobilized monomeric LZ, and K_a is the apparent association constant for LZ* and N-PKG. An algorithm was written using the program ORIGIN to fit the binding curve for LZ, with K_d for the N-PKG dimer and the concentration of N-PKG as fixed inputs, and K_a allowed to float (the details of this analysis will be published elsewhere by K. L. & T.C. T.). The analysis yielded $K_a = 5.3 \times 10^4$ M, or $K_d = 1/K_a = 19(\pm 0.6)$ μM. For the dimeric peptides E_2CCLZ and CCLZ, it is assumed that only one of the two polypeptide chains was covalently attached to the chip. The analysis for these peptides are therefore identical to that for LZ. Fitting of the binding curves of E_2CCLZ and CCLZ yielded $K_d = 25(\pm 1.1)$ μM and $15(\pm 0.9)$ μM, respectively. A summary of all our binding results is presented in Table 2.

Discussion

The serine/threonine kinase PKG is present in all smooth muscles as well as several other tissues at high concentrations (>0.1 μM).[39] In mammals, two separate genes encode PKGI and PKGII, and alternative splicing gives rise to two PKGI isoforms, *viz*. PKGIα and PKGIβ. All three PKG isoforms contain a regulatory and a catalytic domain, and an N-terminal leucine-zipper motif. It has been reported that PKG exists as a dimer and dimerization is mediated by this leucine-zipper motif.[28,40] Our expressed N-PKG peptide (residues 1–47) corresponds to the coiled coil region predicted by MULTICOIL, and contains the leucine-zipper motif (residues 12–47). Our sedimentation velocity results (Table 1; Figure 4) show that N-PKG is dimeric and high in α-helical content, confirming that this N-terminal leucine-zipper motif mediates homodimerization of PKG *via* coiled coil formation.

In contrast to N-PKG, our expressed LZ peptide containing the leucine-zipper motif at the C terminus of MYPT1 is monomeric and has a very low α-helix content, indicating that it does not form a coiled coil by itself. The reason why this is so may be because of the presence of Pro1005 at position 19

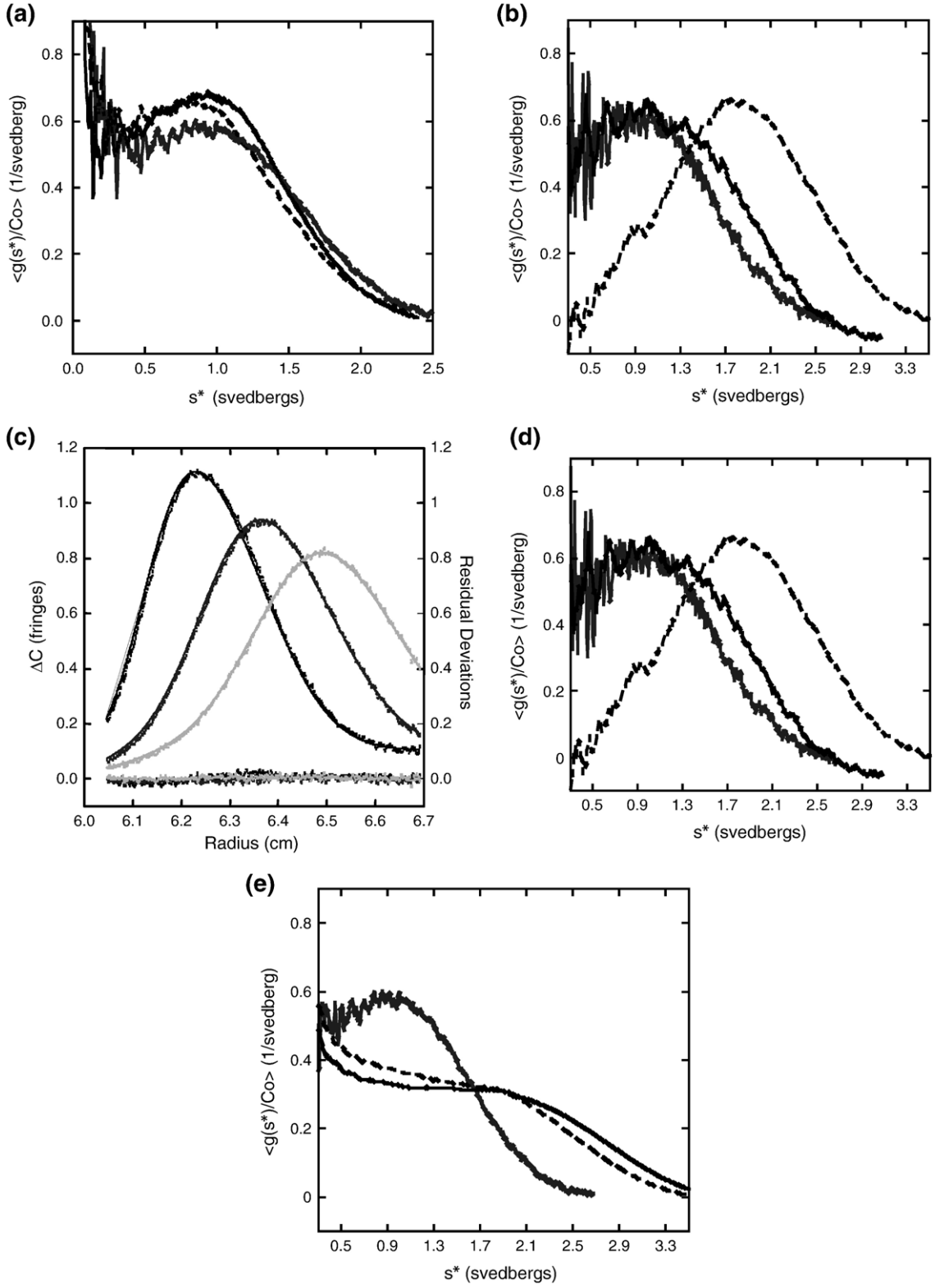

Figure 5. Binding analysis by sedimentation velocity. (a) $g(s^*)$ plots of N-PKG alone at 31.0 μM (gray line), E_1E_2CC alone at 39 μM (broken line), and a mixture of N-PKG and E_1E_2CC at 35 μM each (line). (b) $g(s^*)$ plots of N-PKG alone at 13.6 μM (gray line), E_1E_2CC alone at 2.4 μM (broken line), and a mixture of N-PKG and E_1E_2CC at 4.8 μM each (continuous line). (c) Fitting of time-difference plots for mixtures of N-PKG and E_1E_2CC. A global fit of 2800 total interference scans, 400 each from seven separate experiments on mixtures of the two peptides at different relative concentrations, shows that N-PKG and E_1E_2CC form a heterotetramer. Shown are three representative Δc *versus* radius plots used in the fitting, for a sample of N-PKG and E_1E_2CC at 21.9 μM each. Other captions are the same as for Figure 4(b). (d) $g(s^*)$ plots for N-PKG alone at 13.6 μM (gray line), E_2CCLZ alone at 2.4 μM (broken line), and a mixture of N-PKG and E_2CCLZ at 4.8 μM each (continuous line). (e) $g(s^*)$ plots for N-PKG alone at 41.2 μM (gray line), LZ alone at 179 μM (broken line), and a mixture of N-PKG and LZ at 12.2 and 179 μM, respectively (continuous line).

of the peptide. It divides the peptide into a 14 and a 29 residue N and C-terminal segment, respectively. Both contain heptad repeats (two and four in the N and C-terminal segments, respectively), but it appears that neither is long enough to form a stable coiled coil. For the CCLZ peptide, although the α-helix content decrease from that of the CC peptide, as can be expected when a coiled coil-containing segment (CC) is joined to a non-helical segment (LZ), the number of helical residues increases from 41 in CC to 54 in CCLZ. Inspection of the CCLZ sequence reveals that the two-heptad N-terminal overhang from LZ is contiguous and in phase with the heptad repeats from CC, so that it is very likely that when joined in CCLZ they engage in the formation of additional α-helical coiled coil residues. The residues C-terminal to Pro1005, however, are likely to remain "unzipped" and non-helical. E_1E_2, like LZ, has a very low α-helix content (Figure 2). All the other CC-containing peptides have varying α-helix contents that are lower than that for CC alone, as can be expected when non-helical segments (i.e. LZ, E_1E_2, etc.) are added onto an α-helical segment (i.e. CC). In short, our circular dichroism results show that while N-PKG, CC and the CC-containing peptides all contain significant amounts of α-helical structure, LZ and E_1E_2 are virtually non-helical.

The thermal denaturation properties of N-PKG, CC and three of the CC-containing peptides, E_1E_2CC, CCLZ and E_2CCLZ show that the three CC-containing peptides exhibit reversible thermal denaturation/renaturation with relatively high transition temperatures of 56–59 °C, similar to that for CC by itself (Figure 3(a)), consistent with the notion that denaturation corresponds to unfolding of the α-helical coiled coil segment of CC. For N-PKG freshly treated with 2 mM DTT, only the beginning of a transition could be detected at 70 °C, indicating that this peptide is significantly more stable than the CC-containing peptides. For N-PKG without fresh DTT treatment, no transition could be discerned even at 80 °C. N-PKG has one cysteine residue at position 42, five residues upstream from the C terminus. Our observations could be explained by the formation of an inter-chain disulfide cross-link at Cys42 in oxidized N-PKG, thereby further stabilizing the coiled coil dimer. This implies that N-PKG is a parallel coiled coil, consistent with a recent NMR study showing that the peptide comprising residues 1–59 of PKG is a parallel dimer.[41] No attempt was made to determine the transition midpoint for oxidized N-PKG. The transition midpoint for reduced N-PKG was determined by differential scanning calorimetry to be as high as 94 °C (Figure 3(b)), further illustrating the stability of the N-PKG peptide.

Our velocity analytical ultracentrifugation studies on the individual peptides show that while N-PKG, CC, E_1CC, E_2CC and E_1E_2CC are dimeric, LZ and E_1E_2 are monomeric. As discussed above, our circular dichroism results show that while N-PKG, CC and these three CC-containing peptides contain substantial amounts of α-helix, LZ and E_1E_2 are virtually non-helical. Together, these findings lead us to conclude that whereas N-PKG, CC and these CC-containing peptides are dimers that contain an α-helical coiled coil segment, LZ, E_1, E_2 are most likely unstructured monomers. For the two CC-containing peptides that contain LZ as well, CCLZ and E_2CCLZ, we could not conclude that they are dimers from our analytical ultracentrifugation results owing to oligomerization caused by the LZ segment. However, considering that, like the other CC-containing peptides, they contain substantial amounts of α-helix and melt at roughly the same temperature (see inset, Figure 3(a)), it is likely that they too are dimeric owing to the presence of the α-helical coiled coil CC segment.

Our analytical ultracentrifugation binding studies show that E_2CCLZ binds to N-PKG to form a heterodimer, but E_2CC does not, suggesting that it is the LZ portion in E_2CCLZ that interacts with N-PKG. Our surface plasmon resonance results show that the two LZ-containing peptides, E_2CCLZ and CCLZ, as well as LZ itself bind to N-PKG with roughly the same affinity, providing evidence that it is the LZ portion that is responsible for binding to N-PKG. Our analytical ultracentrifugation studies also show that E_1E_2CC is capable of binding N-PKG even though it lacks the LZ portion, and that the complex is most likely the $(N\text{-}PKG)_2$–$(E_1E_2CC)_2$ heterotetramer. Although we cannot rule out the N-PKG–$(E_1E_2CC)_2$ heterotrimer, we believe it is less likely because it requires the dissociation of the relatively stable $(N\text{-}PKG)_2$ dimer ($K_d = 0.5$ μM) for its formation. It is not clear why E_1E_2CC is capable of binding N-PKG, but E_1CC, E_2CC and E_1E_2 are not. It is possible that N-PKG interacts with both the E_1E_2 and CC segments in E_1E_2CC, but the interactions with each individual segment are too weak to be detectable. It should be noted that our surface plasmon resonance studies finding no binding between E_1E_2CC and N-PKG do not constitute a contradiction. In fact, it is consistent with our presumption that after washing the immobilized MYPT1 peptide on the sensor chips, only monomeric E_1E_2CC remain immobilized, and our analytical ultracentrifugation studies rule out binding between monomeric E_1E_2CC and dimeric N-PKG.

Our results showing that N-PKG binds to LZ and the LZ-containing peptides of MYPT1 (rows 1–5, Table 2) suggest that PKG and full-length mammalian MYPT1 (i.e. the leucine-zipper-containing isoform) interact with each other *via* their N and C-terminal, respectively, leucine-zipper motifs. Our findings are consistent with those of Surks *et al.*,[28] who reported that mutating residues involved in coiled coil formation in the leucine-zipper motifs of MYPT1 and PKG inhibited the binding between these proteins (rows 12 and 13), and that such MYPT1 mutants could not be phosphorylated by PKG. They are also consistent with the observation that PKG-dependent regulation of smooth muscle

contraction is present in embryonic chicken gizzards when the leucine-zipper-containing MYPT1 isoform is expressed, and absent in adult tissues when the leucine-zipper-lacking MYPT1 isoform is expressed.[27]

Our result showing that the MYPT1 peptide E_1E_2CC can bind N-PKG even though the LZ-segment is not present (row 6, Table 2) provides an explanation for the observation that PKG could bind to the leucine-zipper-lacking MYPT1 isoform that was overexpressed in cultured smooth muscle cells[29] (rows 14 and 15). Since this exogenous MYPT1 isoform was overexpressed at levels five to ten times higher than the endogenous MYPT1 without changing the expression levels of the other MLCP subunits, the excess MYPT1 can well be expected to bind to the leucine-zipper motif of PKG *via* the E_1E_2CC region. The physiological role of this interaction, however, is not clear, because the leucine-zipper-deficient MYPT1 isoform is incapable of participating in PKG-dependent regulation of smooth muscle contraction.[27,29] We can suggest two scenarios to account for these observations; either this binding does not occur in an *in situ* setting,

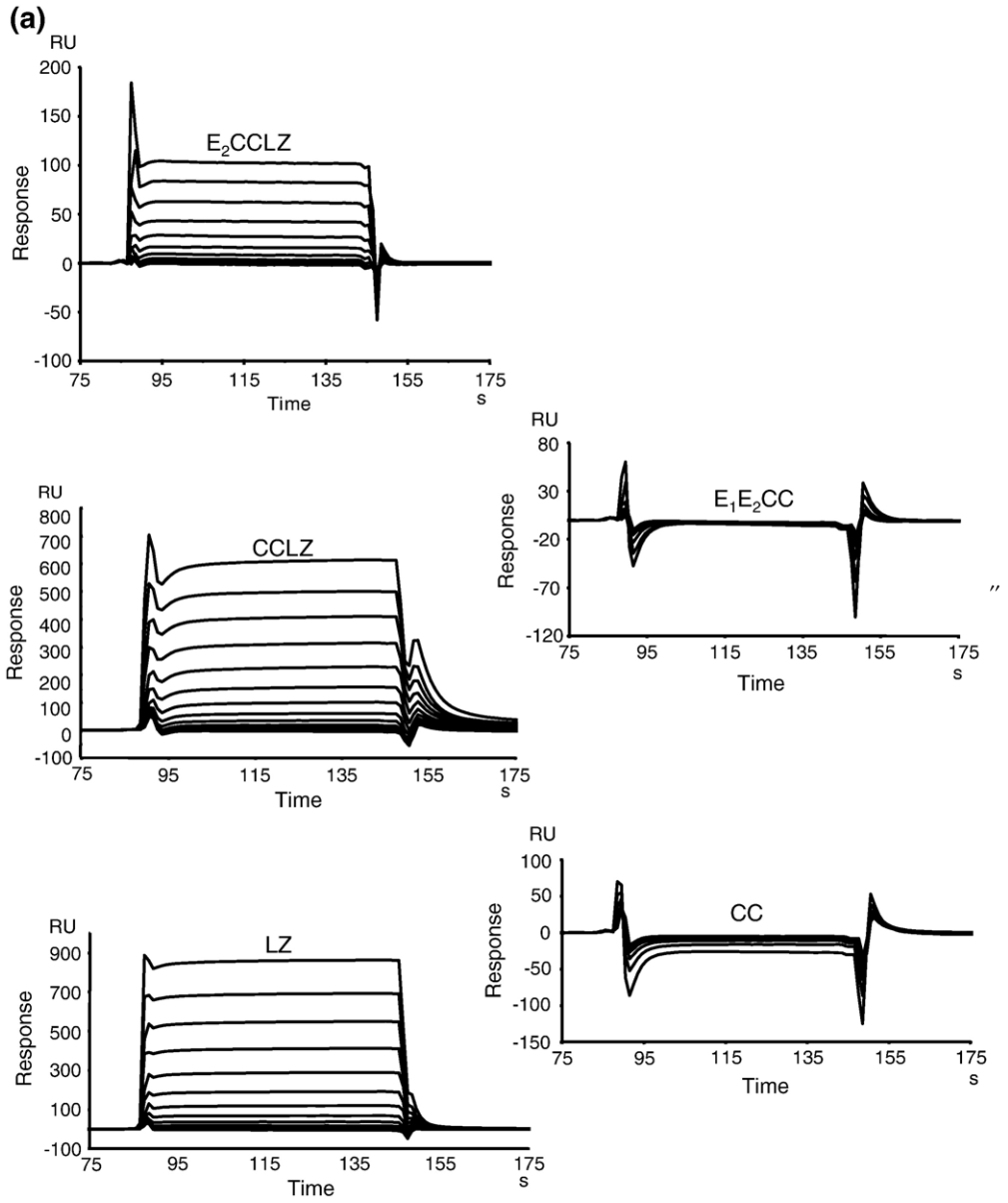

Figure 6. Binding analysis using surface plasmon resonance. (a) Surface plasmon resonance sensorgrams for the interactions of immobilized E_2CCLZ (400 RU), CCLZ (1000 RU), LZ (1000 RU), E_1E_2CC (400 RU), and CC (1000 RU) with N-PKG (0.17-348 μM for E_2CCLZ and E_1E_2CC; 0.14-593 μM for CCLZ, CC, and LZ), after correction for non-specific binding. (b) Fitting of the equilibrium binding curves derived from the data in (a). The equilibrium RU values for each peptide as a function of N-PKG concentration are plotted (filled circles). After modifying the equilibrium binding function to account for the monomer–dimer equilibrium of N-PKG (see Results), a non-linear least-squares best fit to the data (continuous lines) was carried out to determine K_d values using the program Origin 7 (provided by Microcal Inc.).

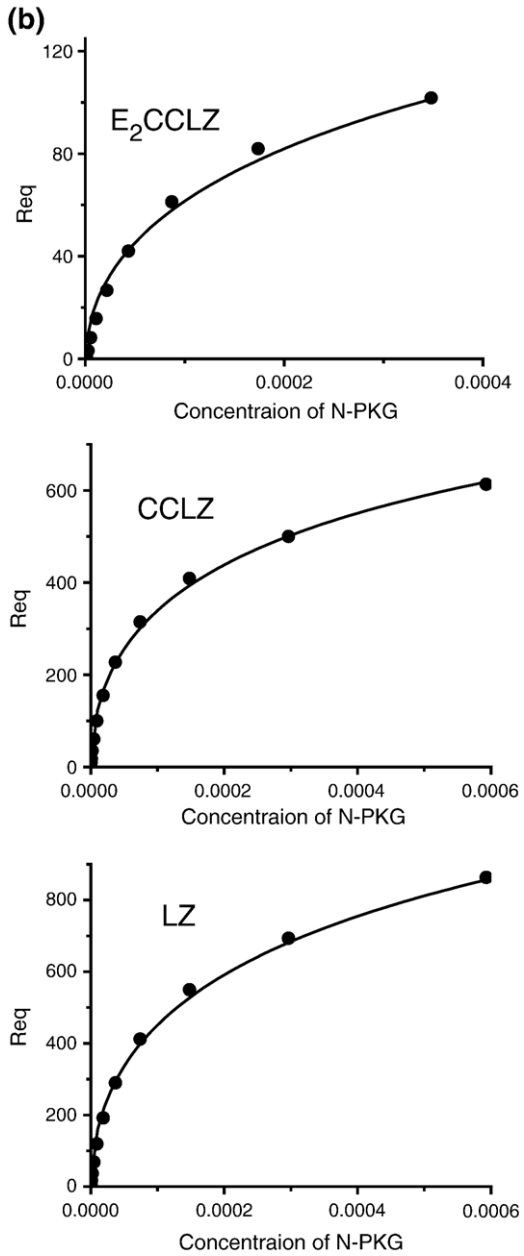

Figure 6 (*legend on previous page*)

or PKG is inactive in this heterotetrameric complex of full-length MYPT1 and PKG. We could not determine K_d for the $(N\text{-}PKG)_2$–$(E_1E_2CC)_2$ complex owing to the presence of heterogeneity in the samples. However, examination of the $g(s^*)$ plot of the 1:1 complex at 9 μM revealed very little dissociation (data not shown), indicating that the K_d value for this complex is ~1 μM or less, a value that does not preclude the formation of this complex *in situ*. For this reason we favor the second scenario, but it is clear that without further experimentation we cannot distinguish these two possibilities.

As discussed above, our results suggest that the E_1E_2 region may be involved in binding N-PKG, and are therefore compatible with the recent report that the residues 888–928 region of MYPT1 (corresponding roughly to the E_2 region of this study) are important for binding PKG.[33] For their studies, Given *et al.*[33] produced four constructs: MYPT1FL, MYPT1TR, MYPT1SO and MYPT1TR2 (the sequences of these constructs and their equivalent designations according to our scheme are shown in Table 2). Our finding that E_2CCLZ binds N-PKG (row 1, Table 2) and that of Surks *et al*. that AL9 binds to PKG (row 10) are compatible with the finding of Given *et al*. that MYPT1FL co-immunoprecipitates with PKG (row 16). Likewise, our finding that the construct with neither the CC nor the LZ segments (i.e. E_1E, row 9) does not bind N-PKG is compatible with the finding of Given *et al*. that MYPT1TR does not co-immunoprecipitate with PKG (row 17). Our finding that E_1E_2CC binds N-PKG (row 6) is also compatible with their finding that MYPT1TR2 binds to PKG (row 19). However, their findings that MYPT1SO, with the E_2 segment deleted (row 18), and the MYPT1FL mutant with two basic residues in the E_2 segment replaced by acidic ones (row 20) do not co-immunoprecipitate with PKG are difficult to reconcile with our results. Although we have not specifically examined equivalent constructs with the E_2 region deleted, nor one with the two basic residues in the E_2 segment converted to acidic ones, our results would predict that since the LZ segment is retained in these constructs, binding to PKG should occur *via* heterodimerization with the latter's leucine-zipper motif. Clearly, further work will be required to reconcile these differences.

We should note that *in situ* the C-terminal region of MYPT1 is presumably complexed with the small subunit of MLCP, M21, and that in principle the interactions of PKG with the MLCP holoenzyme may not be the same as that with the MYPT1 dimer. However, the sequence of M21 reveals that it has corresponding CC and LZ segments at its C terminus, and that the sequences of these segments are 80% homologous to the corresponding segments in MYPT1. Thus, the interactions of PKG with the MLCP holoenzyme are likely to be similar, if not identical to those with the MYPT1 homodimer.

Conclusions

Based on the findings in this study, we conclude the following.

(1) The leucine-zipper motif in human aorta MYPT1 is not likely to be a coiled coil. This may serve to facilitate interactions with MP regulatory proteins with coiled coil regions such as PKG, since uncoiling of the MYPT1 leucine-zipper motif is not needed. In contrast, the coiled coil region in MYPT1 and the leucine-zipper motif in PKG are stable coiled coils.
(2) When it is present, the C-terminal leucine-zipper motif of MYPT1 binds to the N-terminal leucine-zipper motif of PKG, forming a heterodimer.

Table 2. Summary of results derived from binding studies by ourselves and other workers

	MYPT1 constructs	Residues	Binding	Method	Reference
1	E_2CCLZ	892–1030	Yes, heterodimer	AUC[a]	This work
2	〃	892–1030	Yes, $K_d = 25(\pm 1)$ μM	SPR[b]	This work
3	CCLZ	925–1030	Yes, $K_d = 15(\pm 1)$ μM	SPR[b]	This work
4	LZ	992–1030	Yes	AUC[a]	This work
5	LZ	992–1030	Yes, $K_d = 19(\pm 1)$ μM	SPR[b]	This work
6	E_1E_2CC	850–991	Yes, heterotetramer	AUC[a]	This work
7	E_1CC	850–891/924–991	No	AUC[a]	This work
8	E_2CC	892–991	No	AUC[a]	This work
9	E_1E_2	850–924	No	AUC[a]	This work
10	AL9 (E_1E_2CCLZ)[c]	850–1030	Yes	Yeast 2-hybrid/ GST pull-down	Surks *et al.*[32]
11	N-terminal segment	1–690	No	GST-pull-down	Surks*et al.*[32]
12	Full-length L1021A, L1028A	1–1030	No	GST-pull-down	Surks *et al.*[28]
13	Full-length L1007A, L1014A	1–1030	No	GST-pull-down	Surks*et al.*[28]
14	Full-length (LZ+)	1–1039[d]	Yes	IP[e]	Huang *et al.*[29]
15	Full-length (LZ−)	1–1012[d]	Yes	IP[e]	Huang *et al.*[29]
16	MYPT1FL ($E_oE_1E_2$CCLZ)[c]	500–1039[d]	Yes	IP[e]	Given *et al.*[33]
17	MYPT1TR (E_oE_1)[c]	500–890[d]	No	IP[e]	Given *et al.*[33]
18	MYPT1SO (E_oE_1CCLZ)[c]	500–887/929–1039[d]	No	IP[e]	Given *et al.*[33]
19	MYPT1TR2 ($E_oE_1E_2$CC)[c]	500–1010[d]	Yes	IP[e]	Given *et al.*[33]
20	MYPT1FL R916E, K917E	500-1039[d]	No	IP[e]	Given *et al.*[33]

[a] AUC, analytical ultracentrifugation.
[b] SPR, surface plasmon resonance.
[c] Closest designation according to our scheme. E_o designates the 500–887 residues segment.
[d] Chicken aorta MYPT1 numbering.[33]
[e] IP, immunoprecipitation.

Presumably, this interaction leads towards phosphorylation of MYPT1 by PKG, activation of MP and ensuing events that culminate in muscle relaxation. This finding is in agreement with the findings of Surks *et al.*,[28,32] and provides an explanation for the observation that the presence of this motif in MYPT1 is necessary for cGMP-dependent regulation of smooth muscle contraction to be expressed.[27]

(3) When the leucine-zipper motif is not present, the C-terminal region of MYPT1 nevertheless binds to the leucine-zipper motif of PKG, forming a heterotetramer. Evidently, this interaction does not lead towards cGMP-dependent regulation, possibly because either it does not occur *in situ*, or PKG in this heterotetramer is not active. This finding is in agreement with the binding studies of Huang *et al.*, who reported that both the leucine-zipper-present and leucine-zipper-absent isoforms of MYPT1 are capable of binding PKG.[29]

(4) Although our results are in agreement with most of those reported by Given *et al.*, they cannot be reconciled with their finding that deletion of, or mutagenesis within the E_2 segment disrupts PKG binding.[33] Thus, the role of the E_2 segment in the binding of MYPT1 to PKG is still in question. Our current work is focused on characterizing the interactions between PKG and longer C-terminal constructs of MYPT1 with modifications in the E_2 segment.

Materials and Methods

Materials

Unless otherwise specified, materials for SDS–PAGE were from Bio-Rad (Hercules, CA), those for recombinant DNA procedures were from New England BioLabs (Ipswich, MA), a plasmid preparation kit was from Qiagen (Valencia, CA), and buffer components and laboratory chemicals were from Sigma-Aldrich (St. Louis, MO).

Cloning of human PKG cDNA

Human PKGIα cDNA was amplified from a human aorta 5′-stretch cDNA library (Clontech, Mountain View CA) by nested PCR with the primer pair 5′-TGA TTG ACA GCG AGA GGG CTC AGT G and 5′-GAC AGC TTC AGG TTG GCG AAG AAA GCC GC for the primary amplification, and 5′-GTG GAT CCA TGA GCG AGC TAG AGG AAG AC and 5′-GAA TTC TTA GAA GTC TAT ATC CCA TCC TGA for the secondary amplification. The resulting cDNA was sub-cloned into the pCR2.1 vector using the TOPO TA cloning kit (Invitrogen, Carlsbad, CA). Plasmids containing the insert were sequenced at the Tufts University Core Facility, Boston, MA.

Plasmid constructs and primers for PCR

All peptides were sub-cloned into the pTYB12 expression vector (New England BioLabs) to utilize the intein-chitin binding domain affinity purification. The pTYB12/

N-PKG plasmid was constructed by amplifying an N-terminal predicted coiled coil region of PKGIα (amino acids (aa) 6–47) with the primer pair 5′-GGG CAT ATG GAA GAC TTT GCC AAG ATT and 5′-GGG CTC GAG TTA GAG CAC CGA CTG GCA TTT, and fusing it in-frame to the chitin binding domain of pTYB12 vector, utilizing the NdeI/XhoI restriction sites. Various C-terminal regions of MYPT1 were amplified by PCR using the full-length human MYPT1 cDNA as a template with the following primer pairs: E_2CCLZ (aa 891–1030), 5′-GGG CAT ATG GAA ACC AGT TCT ACA TCA GCT and 5′-GGG CTC GAG TTA TTT GGA AAG TTT GCT TAT AAC; CCLZ (aa 924–1030), 5′-AGC CAT ATG CTA GAA AAG GAT GAC TCA ACT G and 5′-CAG GAA TTC TTA TTT GGA AAG TTT GCT; CC (aa 924–990), 5′-AGC CAT ATG CTA GAA AAG GAT GAC TCA ACT G and 5′-GAA TTC TTA TAG AGC TCT TCG TTC CCT T; LZ (aa 991 –1030), 5′-CAT ATG GAA CGT CGT ATC TCT GAA ATG and 5′-CAG GAA TTC TTA TTT GGA AAG TTT GCT; E_1CC (aa 850–890 and aa 930–1003), 5′-ACT GAC TTT AAA AAG CTT TAT GAA CAA ATT CTA and 5′-ATA TCT AGA AAT GGA ATC CGT CTG AGT TTC; E_2CC (aa 891–990), 5′-GGG GGG CAT ATG GAA ACC AGT TCT ACA TCA GCT and 5′-GAA TTC TTA TAG AGC TCT TCG TTC CCT T; E_1E_2 (aa 850 –923), 5′-GGT AGC CAT ATG AGA AGA TCT ACA GGA GTT TCA and 5′-CCC GAA TTC TTA CCT GCT GCT GTA AGG TTT TCT; E_1E_2CC (aa 850–990), 5′-GGT AGC CAT ATG AGA AGA TCT ACA GGA GTT TCA and 5′- GAA TTC TTA TAG AGC TCT TCG TTC CCT T. The amplified fragments were cloned into pTYB12 using the NdeI/EcoRI restriction sites, with the exception of E_2CCLZ cDNA for which the NdeI/XhoI restriction sites were utilized.

Recombinant peptides

The Various MYPT1 peptides and N-PKG were produced in *Escherichia coli* strain BL21(DE3) or KS1000(DE3), and purified according to the manufacturer's protocol. Briefly, cultures in late logarithmic growth phase were induced with 0.3 mM isopropyl-β-D-thiogalactopyranoside at 20 °C overnight. Bacterial pellets were resuspended in 1/100 culture volume of the lysis buffer (20 mM Tris–HCl (pH 8.0), 500 mM NaCl, 1 mM EDTA, and 0.1 %(v/v) Triton X-100) and then sonicated. Recombinant peptides were extracted from cleared lysates by chitin beads (provided by the manufacturer) followed by washes with the washing buffer (20 mM Tris–HCl (pH 8.0), 1 M NaCl, 1 mM EDTA, and 0.1 % Triton X-100). The peptides were cleaved from the chitin binding domain with the cleavage buffer (20 mM Tris–HCl (pH 8.0), 50 mM NaCl, 1 mM EDTA, and 50 mM dithiothreitol (DTT)) at room temperature overnight followed by elution with the column buffer (20 mM Tris–HCl (pH 8.0), 500 mM NaCl, and 1 mM EDTA). Further purification was done by HPLC on a Vydac C8 reversed phase column using an acetonitrile gradient. The purity of each peptide was determined on 16.5% Tris-tricine PAGE, and the identity was verified by mass spectrometry. All recombinant peptides include four residues at the N terminus from the cloning.

Circular dichroism analyses

Circular dichroism spectra and temperature dependence of the ellipticity were recorded on an Aviv 62A DS spectropolarimeter (Aviv Biomedical, Lakewood, NJ) using water-jacketed, dichroically neutral quartz cuvettes with a path length of 1.0 mm. Each peptide was dialyzed against 5 mM potassium phosphate buffer (pH 8.0) containing 10 mM KCl, and 1 mM DTT at 4 °C overnight. Spectra were measured between 260 nm and 190 nm at 25 °C, using a bandwidth of 0.25 nm and a time constant of 0.2 s. Five scans were averaged for each spectrum and then corrected for solvent contribution. Measured rotations were converted to mean residue ellipticity by the following equation:

$$[\Theta]_\lambda = \Theta_\lambda^{obs} \times \frac{1}{10lcn} (\text{deg. cm}^2\ \text{dmol}^{-1}) \qquad (1)$$

where $[\Theta]_\lambda$ is the mean residue ellipticity, Θ_λ^{obs} is the experimentally observed ellipticity, l is the pathlength in cm, c is the concentration, and n is the number of residues in the peptide. The α-helical content was estimated from the mean residue ellipticity by the following equation:

$$\%\alpha - \text{helix} = \frac{[\Theta]_{222nm}^{obs}}{[\Theta]_{222nm}^{100\%}} \times 1000 \qquad (2)$$

where $[\Theta]_{222nm}^{100\%} = -32{,}000$ deg. cm^2 dmol^{-1}.[42] for the thermal denaturation studies the ellipticity at 222 nm was recorded from 10 °C –80 °C using a cuvette with a path length of 1.0 cm, an equilibration time of 0.3 min, a step size of 1 °C, a bandwidth of 1 nm, and an averaging time of 10 s, with constant stirring.

For the N-PKG peptide differential scanning calorimetry was used to further characterize its thermal denaturation. Measurements were made using a MicroCal (Northampton, MA) VP-DSC calorimeter. Data were collected from 10 °C to 120 °C, with heating at a rate of 90 °C/h.

Analytical ultracentrifugation

Individual peptides were dissolved in 50 mM potassium phosphate buffer (pH 8.0) containing 100 mM KCl, and 1 mM DTT and dialyzed against the same buffer overnight. All the peptides, diluted threefold serially, were subjected to sedimentation velocity measurements using a Beckmen Coulter (Fullerton, CA) Optima XL-I Ultracentrifuge equipped with a real-time video-based data acquisition system and Rayleigh optics. Runs were made in an eight-hole rotor at 50,000 rpm at 20 °C, and 999 sedimentation velocity patterns were collected over a total period of 9 h. The program SEDANAL[43] was used for direct boundary fitting to the sedimentation velocity scans. Standard deviations below 0.01 fringes were acceptable for a good fit given the signal-to-noise ratio of the instrument. For the binding studies, a non-interacting model based on successful fits of the individual components was first applied. Models of increasing complexity were then applied until a fit with a standard deviation close to the noise of the system was reached. The program SEDNTERP[44] was used to interpolate buffer density and viscosity, estimate peptide partial specific volume from the sequence, and for shape analysis based on experimentally determined sedimentation coefficients.

Surface plasmon resonance measurements

Surface plasmon resonance measurements were carried out on a Biacore (Uppsala, Sweden) 3000 instrument at 25 °C. Sensor chips and reagents for immobilization, 1-ethyl-3-(3-dimethylaminopropyl) carbodiimide, *N*-

hydroxyl-succinimide and ethanolamine were purchased from Biacore. Peptides were immobilized onto a CM5 sensor chip using the amine coupling method. Typically, 400–1000 resonance units (RU) of peptides were immobilized. Running buffer used was 50 mM potassium phosphate (pH 8.0) containing 100 mM KCl, and 1 mM DTT or Hepes-buffered saline (HBS) containing 10 mM Hepes and 150 mM NaCl (pH 7.4) with 0.005%(v/v) Surfactant P20. Twofold serial dilutions of N-PKG from 348 μM or 593 μM were used for the binding studies. Binding data were obtained by measuring the steady state responses at various concentrations, after correction for non-specific binding. E_1CC and a nebulin-derived peptide were immobilized at similar densities to the MYPT1 peptides to serve as negative control surfaces.

Acknowledgements

We thank Dr Walter F. Stafford III for critically reviewing the manuscript. We thank Dr Masaaki Ito for the generous gift of a human MYPT1 clone. This work was supported by National Institutes of Health grants P01 AR41637 and R01 AR49066.

References

1. Hartshorne, D. J. (1987). Biochemistry of the contractile process in smooth muscle. In *Physiology of the Gastrointestinal Tract* (Johnson, L. R., ed), pp. 423–481,.
2. Kanaide, H. (1998). In *Methods in Molecular Biology* (Lambert, D. G., ed), pp. 269–277, Humana Press Inc, Totowa, NJ.
3. Hirano, K., Hirano, M., Abe, S. & Kanaide, H. (1991). In *Ion Channels of Vascular Smooth Muscle Cells and Endothelial Cells* (Sperelakis, N. & Kuriyama, H., eds), pp. 93–105, Elsevier, New York.
4. Somlyo, A. P. & Somlyo, A. V. (1994). Signal transduction and regulation in smooth muscle. *Nature*, **372**, 231–236.
5. Morgan, J. P. & Morgan, K. G. (1984). Stimulus-specific patterns of intracellular calcium levels in smooth muscle of ferret portal vein. *J. Physiol.* **351**, 155–167.
6. Hartshorne, D. J., Ito, M. & Erdodi, F. (1998). Myosin light chain phosphatase: subunit composition, interactions and regulation. *J. Muscle Res. Cell Motil.* **19**, 325–341.
7. Hartshorne, D. J., Ito, M. & Erdodi, F. (2004). Role of protein phosphatase type 1 in contractile functions: myosin phosphatase. *J. Biol. Chem.* **279**, 37211–37214.
8. Kimura, K., Ito, M., Amano, M., Chihara, K., Fukata, Y., Nakafuku, M. *et al.* (1996). Regulation of myosin phosphatase by Rho and Rho-associated kinase (Rho-kinase). *Science*, **273**, 245–248.
9. Masuo, M., Reardon, S., Ikebe, M. & Kitazawa, T. (1994). A novel mechanism for the Ca(2+)-sensitizing effect of protein kinase C on vascular smooth muscle: inhibition of myosin light chain phosphatase. *J. Gen. Physiol.* **104**, 265–286.
10. Gong, M. C., Fuglsang, A., Alessi, D., Kobayashi, S., Cohen, P., Somlyo, A. V. & Somlyo, A. P. (1992). Arachidonic acid inhibits myosin light chain phosphatase and sensitizes smooth muscle to calcium. *J. Biol. Chem.* **267**, 21492–21498.
11. Li, L., Eto, M., Lee, M. R., Morita, F., Yazawa, M. & Kitazawa, T. (1998). Possible involvement of the novel CPI-17 protein in protein kinase C signal transduction of rabbit arterial smooth muscle. *J. Physiol.* **508**, 871–881.
12. Eto, M., Kitazawa, T., Yazawa, M., Mukai, H., Ono, Y. & Brautigan, D. L. (2001). Histamine-induced vasoconstriction involves phosphorylation of a specific inhibitor protein for myosin phosphatase by protein kinase C alpha and delta isoforms. *J. Biol. Chem.* **276**, 29072–29078.
13. Araki, S., Ito, M., Kureishi, Y., Feng, J., Machida, H., Isaka, N. *et al.* (2001). Arachidonic acid-induced Ca^{2+} sensitization of smooth muscle contraction through activation of Rho-kinase. *Pflugers Arch.* **441**, 596–603.
14. Wang, G. R., Zhu, Y., Halushka, P. V., Lincoln, T. M. & Mendelsohn, M. E. (1998). Mechanism of platelet inhibition by nitric oxide: in vivo phosphorylation of thromboxane receptor by cyclic GMP-dependent protein kinase. *Proc. Natl. Acad. Sci. USA*, **95**, 4888–4893.
15. Cornwell, T. L., Pryzwansky, K. B., Wyatt, T. A. & Lincoln, T. M. (1991). Regulation of sarcoplasmic reticulum protein phosphorylation by localized cyclic GMP-dependent protein kinase in vascular smooth muscle cells. *Mol. Pharmacol.* **40**, 923–931.
16. Ammendola, A., Geiselhoringer, A., Hofmann, F. & Schlossmann, J. (2001). Molecular determinants of the interaction between the inositol 1,4,5-trisphosphate receptor-associated cGMP kinase substrate (IRAG) and cGMP kinase Ibeta. *J. Biol. Chem.* **276**, 24153–24159.
17. Geiselhoringer, A., Werner, M., Sigl, K., Smital, P., Worner, R., Acheo, L. *et al.* (2004). IRAG is essential for relaxation of receptor-triggered smooth muscle contraction by cGMP kinase. *EMBO J.* **23**, 4222–4231.
18. Komalavilas, P. & Lincoln, T. M. (1994). Phosphorylation of the inositol 1,4,5-trisphosphate receptor by cyclic GMP-dependent protein kinase. *J. Biol. Chem.* **269**, 8701–8707.
19. Schlossmann, J., Ammendola, A., Ashman, K., Zong, X., Huber, A., Neubauer, G. *et al.* (2000). Regulation of intracellular calcium by a signalling complex of IRAG, IP3 receptor and cGMP kinase Ibeta. *Nature*, **404**, 197–201.
20. Alioua, A., Tanaka, Y., Wallner, M., Hofmann, F., Ruth, P., Meera, P. & Toro, L. (1998). The large conductance, voltage-dependent, and calcium-sensitive K^+ channel, Hslo, is a target of cGMP-dependent protein kinase phosphorylation in vivo. *J. Biol. Chem.* **273**, 32950–32956.
21. White, R. E., Lee, A. B., Shcherbatko, A. D., Lincoln, T. M., Schonbrunn, A. & Armstrong, D. L. (1993). Potassium channel stimulation by natriuretic peptides through cGMP-dependent dephosphorylation. *Nature*, **361**, 263–266.
22. Fukao, M., Mason, H. S., Britton, F. C., Kenyon, J. L., Horowitz, B. & Keef, K. D. (1999). Cyclic GMP-dependent protein kinase activates cloned BKCa channels expressed in mammalian cells by direct phosphorylation at serine 1072. *J. Biol. Chem.* **274**, 10927–10935.
23. Schmidt, H. H., Lohmann, S. M. & Walter, U. (1993). The nitric oxide and cGMP signal transduction system: regulation and mechanism of action. *Biochim. Biophys. Acta*, **1178**, 153–175.
24. Wu, X., Somlyo, A. V. & Somlyo, A. P. (1996). Cyclic GMP-dependent stimulation reverses G-protein-coupled inhibition of smooth muscle myosin light chain phosphate. *Biochem. Biophys. Res. Commun.* **220**, 658–663.

25. Lee, M. R., Li, L. & Kitazawa, T. (1997). Cyclic GMP causes Ca^{2+} desensitization in vascular smooth muscle by activating the myosin light chain phosphatase. *J. Biol. Chem.* **272**, 5063–5068.
26. Etter, E. F., Eto, M., Wardle, R. L., Brautigan, D. L. & Murphy, R. A. (2001). Activation of myosin light chain phosphatase in intact arterial smooth muscle during nitric oxide-induced relaxation. *J. Biol. Chem.* **276**, 34681–34685.
27. Khatri, J. J., Joyce, K. M., Brozovich, F. V. & Fisher, S. A. (2001). Role of myosin phosphatase isoforms in cGMP-mediated smooth muscle relaxation. *J. Biol. Chem.* **276**, 37250–37257.
28. Surks, H. K. & Mendelsohn, M. E. (2003). Dimerization of cGMP-dependent protein kinase 1alpha and the myosin-binding subunit of myosin phosphatase: role of leucine zipper domains. *Cell Signal.* **15**, 937–944.
29. Huang, Q. Q., Fisher, S. A. & Brozovich, F. V. (2004). Unzipping the role of myosin light chain phosphatase in smooth muscle cell relaxation. *J. Biol. Chem.* **279**, 597–603.
30. Nakamura, M., Ichikawa, K., Ito, M., Yamamori, B., Okinaka, T., Isaka, N. *et al.* (1999). Effects of the phosphorylation of myosin phosphatase by cyclic GMP-dependent protein kinase. *Cell Signal.* **11**, 671–676.
31. Wooldridge, A. A., MacDonald, J. A., Erdodi, F., Ma, C., Borman, M. A., Hartshorne, D. J. & Haystead, T. A. (2004). Smooth muscle phosphatase is regulated in vivo by exclusion of phosphorylation of threonine 696 of MYPT1 by phosphorylation of Serine 695 in response to cyclic nucleotides. *J. Biol. Chem.* **279**, 34496–34504.
32. Surks, H. K., Mochizuki, N., Kasai, Y., Georgescu, S. P., Tang, K. M., Ito, M. *et al.* (1999). Regulation of myosin phosphatase by a specific interaction with cGMP-dependent protein kinase Ialpha. *Science*, **286**, 1583–1587.
33. Given, A. M., Ogut, O. & Brozovich, F. V. (2007). MYPT1 mutants demonstrate the importance of aa 888-928 for the interaction with PKGIa. *Am. J. Physiol. Cell. Physiol.* **292**, C432–C439.
34. Wolf, E., Kim, P. S. & Berger, B. (1997). MultiCoil: a program for predicting two- and three-stranded coiled coils. *Protein Sci.* **6**, 1179–1189.
35. Langsetmo, K., Stafford, W. F., Mabuchi, K. & Tao, T. (2001). Recombinant small subunit of smooth muscle myosin light chain phosphatase - Molecular properties and interactions with the targeting subunit. *J. Biol. Chem.* **276**, 34318–34322.
36. Wang, C.-L. A., Chalovich, J. M., Graceffa, P., Lu, R. C., Mabuchi, K. & Stafford, W. F. (1991). A long helix from the central region of smooth muscle caldesmon. *J. Biol. Chem.* **266**, 13958–13963.
37. Freire, E. (1995). Thermal denaturation methods in the study of protein folding. *Methods Enzymol.* **259**, 144–168.
38. Gomez, J., Hilser, V. J., Xie, D. & Freire, E. (1995). The heat capacity of proteins. *Proteins: Struct. Funct. Genet.* **22**, 404–412.
39. Hofmann, F. (2005). The biology of cyclic GMP-dependent protein kinases. *J. Biol. Chem.* **280**, 1–4.
40. Richie-Jannetta, R., Busch, J. L., Higgins, K. A., Corbin, J. D. & Francis, S. H. (2006). Isolated regulatory domains of cGMP-dependent protein kinase ialpha and Ibeta retain dimerization and native cGMP-binding properties and undergo isoform-specific conformational changes. *J. Biol. Chem.* **281**, 6977–6984.
41. Schnell, J. R., Zhou, G. P., Zweckstetter, M., Rigby, A. C. & Chou, J. J. (2005). Rapid and accurate structure determination of coiled-coil domains using NMR dipolar couplings: application to cGMP-dependent protein kinase Ialpha. *Protein Sci.* **14**, 2421–2428.
42. Wu, C. S., Ikeda, K. & Yang, J. T. (1981). Ordered conformation of polypeptides and proteins in acidic dodecyl sulfate solution. *Biochemistry*, **20**, 566–570.
43. Stafford, W. F. & Sherwood, P. J. (2004). Analysis of heterologous interacting systems by sedimentation velocity: curve fitting algorithms for estimation of sedimentation coefficients, equilibrium and rate constants. *Biophys. Chem.* **108**, 231–243.
44. Laue, T. M., Shah, B. D., Ridgeway, T. M. & Pelletier, S. (1992). *Computer-aided interpretation of analytical sedimentation data for proteins.* Analytical Ultracentrifugation in Biochemistry and Polymer Science Redwood Press Ltd, Melksham, UK.